Available online at www.sciencedirect.com
SCIENCE DIRECT®
Surface and Coatings Technology 172 (2003) 242–250
SURFACE & COATINGS TECHNOLOGY
www.elsevier.com/locate/surfcoat

Structural and optical properties of indium oxide thin films prepared by an ultrasonic spray CVD process

Mihaela Girtan[a,*], G. Folcher[b]

[a]*Solid State Department, 'Al.I. Cuza' University, Bd. Carol I no 11, Iasi, 6600, Romania*
[b]*Laboratoire de Physique des Liquides et Electrochimie, UPR15-CNRS, Universite 'Pierre et Marie Curie', 4 Place Jussieu, F75252 Paris Cedex 05, France*

Received 11 October 2002; accepted in revised form 7 February 2003

Abstract

Polycrystalline In_2O_3 thin films have been synthesized by a modified chemical vapor deposition process using the pyrolysis of an aerosol generated by ultrahigh frequency spraying of a volatile precursor solution. The deposition has been carried out on glass substrates (350–550 °C). X-Ray diffraction has shown that deposited films are polycrystalline without second phases. The morphology of the surface as function of the substrate temperature has been studied using scanning electron microscopy (LEO Stereoscan 440). Transmission and reflection spectra of the sprayed films were examined in the 260–2600 nm spectral range and, for investigated films, the transmission coefficient in the visible and infrared regions exceed 85% and is weakly affected by deposition temperature. The optical band gap values, E_g, ranged between 3.57 and 3.68 eV. The Urbach tail parameter E_0, was calculated for films deposited at different temperatures.

Keywords: Indium oxide; Chemical vapor deposition; X-Ray diffraction; Scanning electron microscopy; Transmission

1. Introduction

It is known that indium oxide (IO) thin films are important semiconductor materials with wide band gap, good chemical stability and transparency to visible light. Therefore, they are frequently used for photovoltaic devices [1], in biological systems [2] and in a variety of electro-optical devices such as flat panel display devices and heat reflecting mirrors [3–5]. A variety of deposition techniques such as evaporation [6–8], reactive thermal deposition [9–12], electron beam evaporation [13,14], sputtering [15–17] and spray pyrolysis [18–21] have been used for the preparation of doped and undoped indium oxide thin films. In this paper we report the results of a study involving other spraying method. We use ultrasonic vibration to atomize the solution in advance, then spray it to form films on sheets (pyrosol technique [22–24]). In the pyrosol process the droplet size is very small and does not have a wide distribution. Since the carrier gas is used only to direct the aerosol into the reaction zone a lower flow can be used, which reduces the effect of substrate cooling. In our previous paper [25] we distinguished the advantages of pyrosol technique compared with the pneumatic spray process for the deposition of indium oxide thin films (improvement of the quality of thin films, reduction of their preparation cost by increasing the efficiency of the spraying method, decrease of deposition temperature).

Theoretical studies made by Portier et al. [26] showed that, besides tin, other doping elements could be suitable to obtain high conductive doped indium oxide thin films. As the chemical methods are very practical to produce doped films, we considered that is important to monitor first, the properties of undoped indium oxide thin films. However, although indium tin oxide (ITO) is an intensively studied material, very little work has been reported on undoped indium oxide thin films.

*Corresponding author. Tel.: +40-32-201136; fax: +40-32-201150.
E-mail address: girtan@uaic.ro (M. Girtan).

0257-8972/03/$ - see front matter © 2003 Elsevier Science B.V. All rights reserved.
doi:10.1016/S0257-8972(03)00334-7

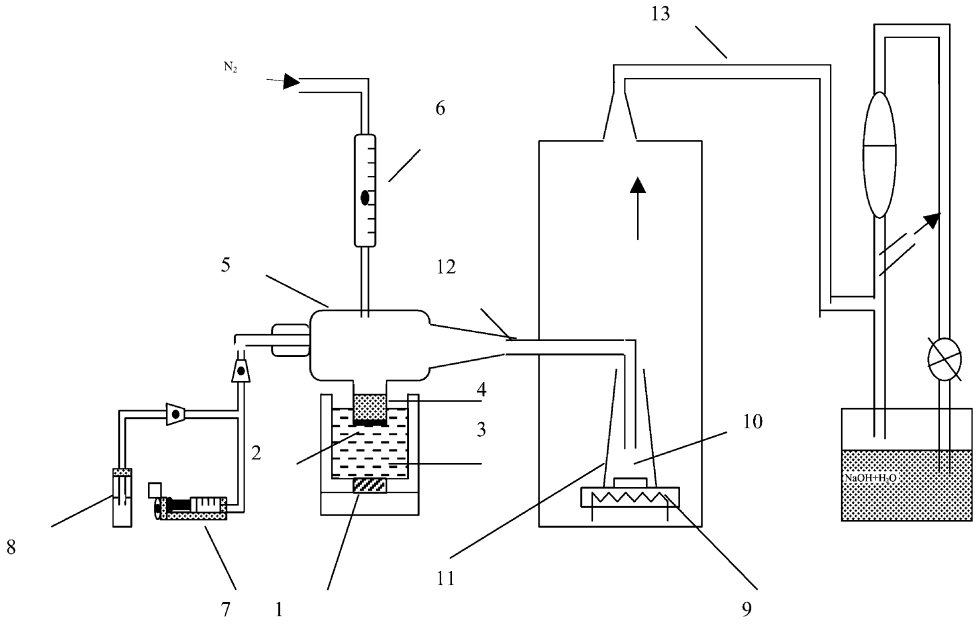

Fig. 1. Apparatus for the pyrosol process: 1, ultrasonic vibrator; 2, glass membrane; 3, water; 4, solution; 5, atomization chamber; 6, gas flowmeter; 7,8, system for maintaining the constant level of spraying solution; 9, heating plate; 10, substrate; 11, pyrolysis reactor; 12, nozzle; 13, exhaust.

2. Experimental

2.1. Deposition process

The spraying method is based on the reversible endothermic reaction [27]:

$$InCl_3 + 3H_2O \leftrightarrow In_2O_3 + 6HCl$$

Water is the most convenient oxidizing agent but the solution is usually diluted with methanol (CH_3OH) or ethanol (C_2H_5OH). The solution used for the films investigated here had the following concentration, expressed in weight percent: 3.5% $InCl_3 \cdot 4H_2O$ (Fulka 99.9%), 26.5% H_2O (distilled), 70% CH_3OH (Merck 99.5%).

The ultrasonic spraying system was developed at the Laboratory UPR15-CNRS, Paris, France (Fig. 1). The ultrasonic vibrator frequency was 824 kHz and the power used was 40 W. To protect the crystal oscillator from erosion and to avoid contamination we used other containers for the spraying solution. A glass membrane separated these two containers. To conserve the spray flow rate magnitude, the height of liquid was maintained constant by adding solution quantities, constantly, during the deposition. The ultrasonic vibrator can produce micronic drops, which form a dense stream. The atomized solution was transported using a carrier gas (Nitrogen or air) onto heated substrates. The carrier gas, used in this case was nitrogen and for all experiments we maintained a gas flow rate, which we found to be suitable to obtain the best quality of the films, of approximately 1.6 l/min.

Films were deposited onto microscope cover glass substrates in the temperature range: 350–550 °C and the deposition time was varied between 10 and 30 min. The substrate temperature was monitored with a thermocouple and controlled electronically. The deposition rate was approximately 1 Å/s.

The resulted waste gases were removed by an extraction pump and passed through a scrubber.

2.2. Measurements

The structure of the films was determined by X-ray diffraction measurements with CuKα radiation from a Philips (type PW 1120/00, No. Dy 813) X-ray generator, operating at 20 mA and 40 kV. The film morphology was examined using a (LEO Stereoscan 440) scanning electron microscope. The composition analysis of the films was performed by energy dispersive analysis of X-ray system (TRACOR) coupled to the scanning electron microscope. The thickness, *d*, of thin films was determined: (i) using an interferential microscope MII 4 [28,29]; and (ii) from the cross-sectional scanning electron micrographs.

The transmittance and reflectance of indium oxide thin films were measured using a Hitachi UV-4001 spectrophotometer in the 260–2600 nm spectral range.

3. Results and discussion

3.1. Structure

X-Ray diffraction analysis, obtained for 2θ scans between 20° and 70°, indicated that the deposited films

Table 1
X-Ray study results for samples deposited at (a) 350 °C, (b) 400 °C, (c) 450 °C, (d) 500 °C

SI. No	Sample	Observed 2θ from XRD (deg)	Standard 2θ (deg)	d_{hkl} exp. (Å)	d_{hkl} standard (Å)	h	k	l
1	(a)	30.55	30.59	2.925	2.921	2	2	2
2		35.35	35.48	2.538	2.529	4	0	0
3		50.90	51.06	1.793	1.788	4	4	0
4		60.55	60.70	1.528	1.525	6	2	2
1	(b)	30.57	30.59	2.923	2.921	2	2	2
2		35.20	35.48	2.548	2.529	4	0	0
3		50.80	51.06	1.796	1.788	4	4	0
4		60.35	60.70	1.533	1.525	6	2	2
1	(c)	30.55	30.59	2.925	2.921	2	2	2
2		35.40	35.48	2.534	2.529	4	0	0
3		50.90	51.06	1.793	1.788	4	4	0
4		60.60	60.70	1.527	1.525	6	2	2
1	(d)	30.55	30.59	2.925	2.921	2	2	2
2		31.65 (NaCl)	31.70	2.825	2.820	2	0	0
3		66.10 (NaCl)	66.22	1.413	1.410	4	0	0

were polycrystalline and retained a cubic bixbyte structure.

Investigated IO films show a slightly (222) preferred orientation which does not change with the variation of deposition temperature. This behavior is different from that observed for ITO-sprayed films [24]. The difference may be due to the fact that the growth mechanisms and consequently the structural properties depend on the concentration of precursor solution used [30], or due to the lower thicknesses of our films [31].

From Table 1 and Table 2 it can be seen that the distances between the crystalline planes are higher than the respective standard values taken from the powder diffraction files. That indicates a compressive stress in all the films [32–34] and we assumed this to the kinetic of the growing process, which is determined by a series of parameters as time, temperature, nature and quantities of atoms involved near the deposition surface.

Fig. 2 corresponds to the films deposited at different substrate temperature and Fig. 3 corresponds to the films deposited at 400 °C for different spraying times (10–30 min). Incidentally, the hump between $2\theta = 20°$ and 30° is due to the background of the glass substrates. For samples deposited from 350 to 500 °C, the increase of temperature leads to an improvement of crystallinity.

Energy dispersive analysis of X-rays (EDAX) generated by the incident electron beam were carried out to investigate the composition of indium oxide films formed. Films deposited under 500 °C are pure indium oxide thin films and no traces of other elements were observed. Contrary to samples deposited at higher temperature (550 °C) a great quantity of NaCl was identified (by X-ray diffraction and EDAX) in the films. We attribute this effect to the diffusion, at higher temperature [27], of alkali ions from the substrate.

Table 2
X-Ray study results for samples deposited at 400 °C for different times

SI. No	Sample	Observed 2θ from XRD (deg)	Standard 2θ (deg)	d_{hkl} exp. (Å)	d_{hkl} standard (Å)	h	k	l
1	(NI19) 10 min	30.50	30.59	2.929	2.921	2	2	2
1	(NI21) 20 min	21.35	–	4.160	–	4	1	0
2		30.45	30.59	2.934	2.921	2	2	2
3		35.32	35.48	2.540	2.529	4	0	0
4		50.85	51.06	1.794	1.788	4	4	0
5		60.45	60.70	1.530	1.525	6	2	2
1	(NI23) 30 min	21.30	–	4.169	–	4	1	0
2		30.50	30.59	2.929	2.921	2	2	2
3		35.38	35.48	2.536	2.529	4	0	0
4		37.61	37.70	2.390	2.385	4	1	1
5		50.90	51.06	1.793	1.788	4	4	0
6		60.60	60.70	1.527	1.525	6	2	2

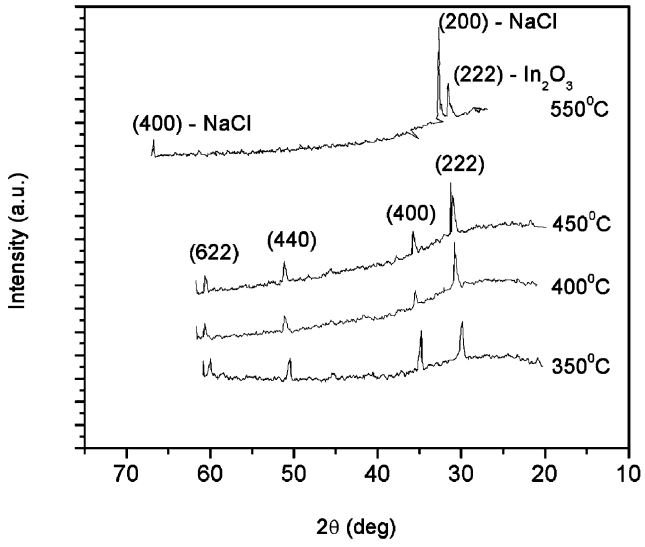

Fig. 2. The XRD patterns of indium oxide thin films deposited at different substrate temperature having thicknesses of approximately 160–170 nm.

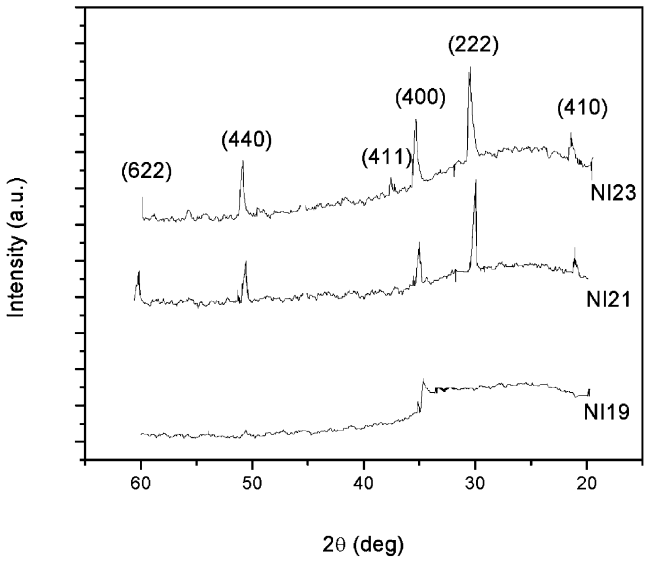

Fig. 3. The XRD patterns of indium oxide thin films deposited at 400 °C for different times: NI 19–10 min, ~40 nm; NI 21–20 min, ~130 nm; NI 23–30 min, ~177 nm.

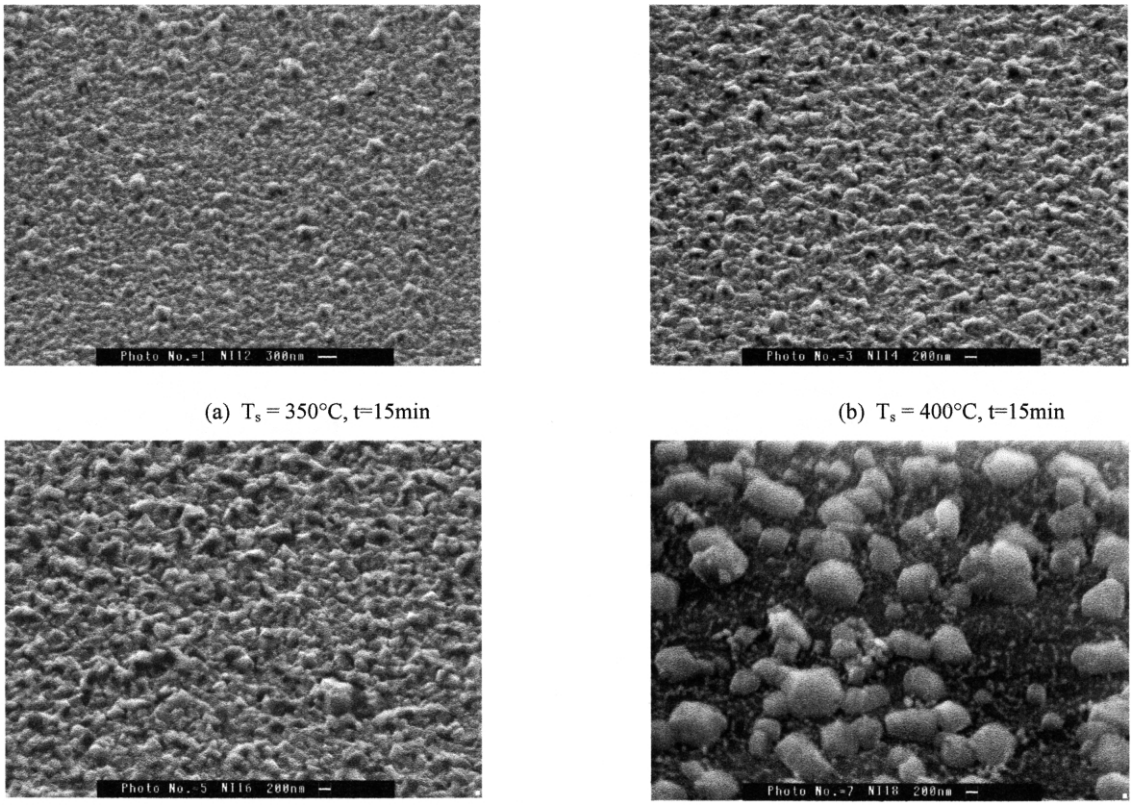

Fig. 4. SEM photographs of indium oxide thin films deposited at different substrate temperatures.

Since the optimal deposition temperature to obtain films with high transparency and electrical conductivity is approximately 450 °C (see below), the fact that the alkali ions diffusion occurs at temperatures as high as 550 °C is only of practical importance.

These results are consistent with those of scanning electron micrographs (SEM) used to examine the surface morphology of indium oxide thin films. Fig. 4 shows the morphology of the sprayed films deposited at different temperatures. It is shown that there is a difference in grain size between the films deposited at different temperatures. The grains of the films increases with increasing of the substrate temperature.

The crystallites observed in Fig. 4d, for films deposited at 550 °C, were identified by EDAX as NaCl.

For thicker films deposited at 400 °C (Fig. 3), a small reflection peak is observed, presumably in the [410] direction, in addition to the peaks corresponding to the card for cubic In_2O_3 (No. ASTM 6-0416). This additional peak is probably due to a deviation from the cubic symmetry.

Fig. 5 shows how the indium oxide films grow with the increase of deposition time. Table 3 summarizes the physical features of films including: the average grain size (D), the average peak-to-valley roughness height (δh), the film thickness as scaled from the micrographs (d_{SEM}) and the film thickness obtained by microinterferometry ($d_{interferometry}$).

Table 3
Films micro-structure data from SEM examinations; the average grain size (D), the average peak-to-valley roughness height (δh), the film thickness as scaled from the micrographs (d_{SEM}) and the film thickness obtained by microinterferometry ($d_{interferometry}$)

Film	D (nm)	δh (nm)	d_{SEM} (nm)	$d_{interferometry}$ (nm)
NI19	120	15	40	47
NI21	400	55	129	135
NI23	500	110	177	178

3.2. Optical properties

The transmittance and reflectance spectra of IO films were measured for films deposited at different temperatures. We investigated: (i) the transmission coefficient; (ii) the optical band gap energy; and (iii) the tail at the absorption edge of undoped indium oxide films of constant thickness. Fig. 6 shows the transmission and reflection vs. wavelength for layers deposited at different

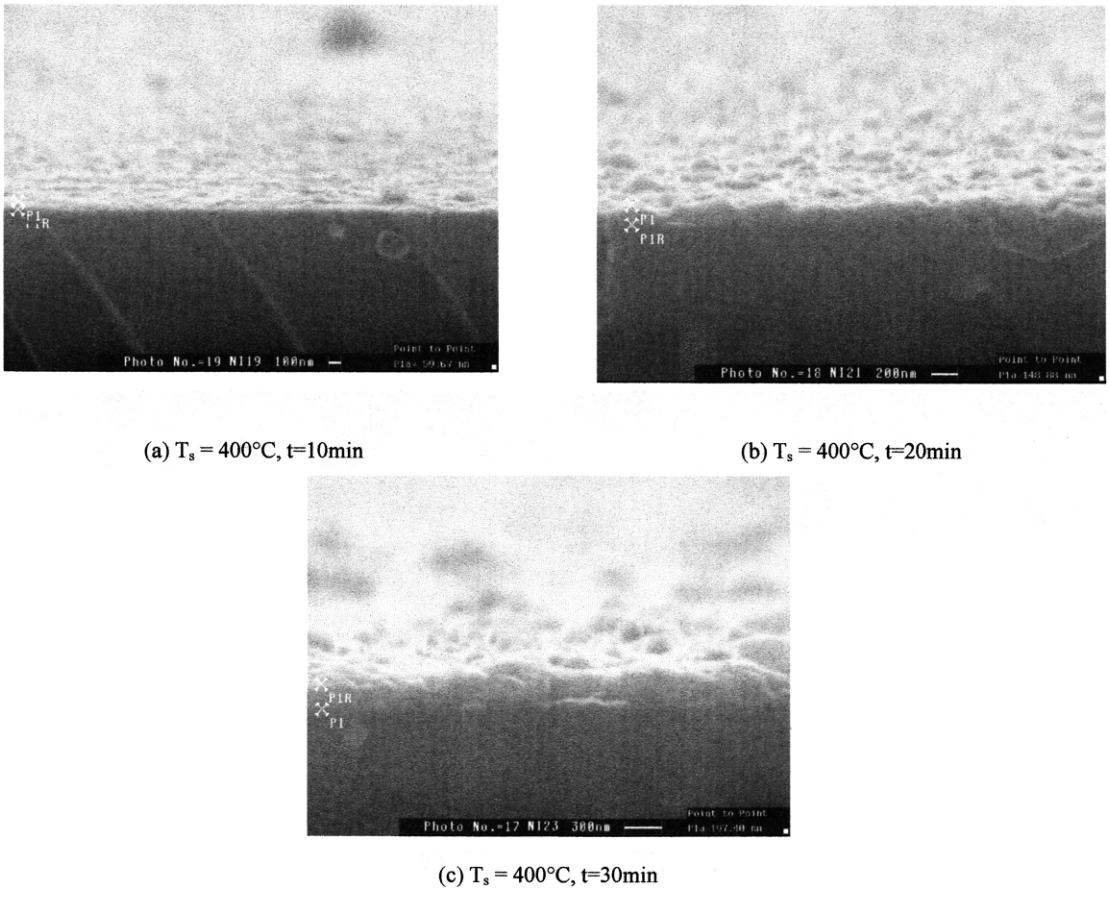

(a) T_s = 400°C, t=10min

(b) T_s = 400°C, t=20min

(c) T_s = 400°C, t=30min

Fig. 5. SEM photographs of indium oxide thin films in transversal section deposited at 400 °C for different times.

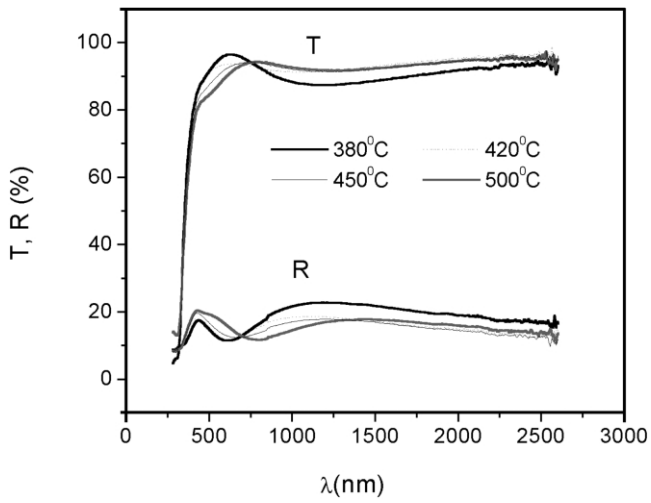

Fig. 6. The transmittance T and reflectance R of indium oxide thin films deposited at different substrate temperatures as a function of wavelength.

temperatures. It is seen from the plots that all the films are highly transparent over the visible and infrared regions. The transmission of such films was not strongly affected by the deposition temperature between 380 and 500 °C and was approximately 85–90%.

The absorption coefficient was calculated using the formula [35]:

$$\alpha(\lambda)=\frac{1}{d}\ln\left[\frac{(1-R(\lambda))^2}{T(\lambda)}\right] \quad (1)$$

where d is the film thickness, R and T are the reflectance and transmittance coefficients, respectively.

Fig. 7 shows the absorption coefficient vs. photon energy, $h\nu$, of samples deposited at different temperatures.

The spectral dependence of α exhibits two regions: a power law region at high photon energies and an exponential absorption region at intermediate energies. If a parabolic density of states is assumed for valence and conduction bands one would expect, for photon energy $h\nu$ greater than the energy gap E_g, the absorption coefficient to vary as:

$$\alpha(h\nu)=C\frac{(h\nu-E_g)^n}{h\nu} \quad (2)$$

where n is a power factor generally being approximately 2. This empirical relation was first derived by Tauc [36] to determine the energy gap, E_g of indirect band gap materials. For direct transition materials, $\alpha(h\nu)$ is given by:

$$\alpha(h\nu)=A(h\nu-E_g)^{1/2} \quad (3)$$

At intermediate photon energy range, we have assumed that the spectral dependence of the absorption edge follows the empirical Urbach rule given by [37]:

$$\alpha(h\nu)=\alpha_0\exp\left(\frac{h\nu-E_1}{E_0}\right) \quad (4)$$

where α_0 is the Urbach absorption at the edge E_1 and E_0 is the Urbach energy width, both obtained from the exponential band-tail absorption. The exponential absorption dependence in the Urbach region ($h\nu<E_g$), is produced by the perturbation of the parabolic density of states at the band edge. The extension of either valence band or conduction band or both into the energy gap in an exponential form is responsible for this Urbach region.

Under various conditions In_2O_3 is a non-stoichiometric compound, with an In/O ratio larger than 2/3. This non-stoichiometry results in a n-type semiconductor or even a semi-metal at high electron concentration. During crystal growth a large number of native donors is produced because of oxygen vacancies. At low concentration, the stoichiometric defects introduce donor levels below the conduction band. At high donor concentrations an impurity band is formed which overlaps the bottom of the conduction band.

The tails in optical absorption spectra of indium oxide thin films can be due to the following [38]: (i) the broadening of impurity levels due to their spatial overlap into the conduction band; (ii) the non-homogeneous distribution of the impurities.

For investigated films, the validity of Eq. (3) has been proved in the absorption range corresponding to $3.7<h\nu<4$ eV and the validity of Eq. (4) in the range $3<h\nu<3.7$ eV. By using Eq. (3) for the direct allowed

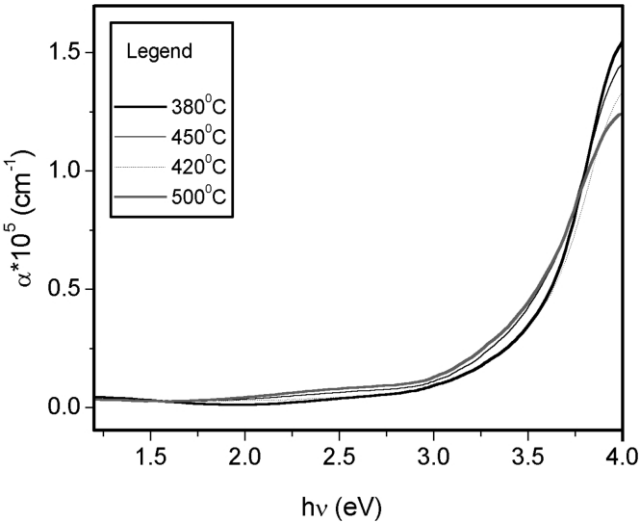

Fig. 7. Absorption coefficient vs. photon energy for polycrystalline thin indium oxide films deposited at different substrate temperatures.

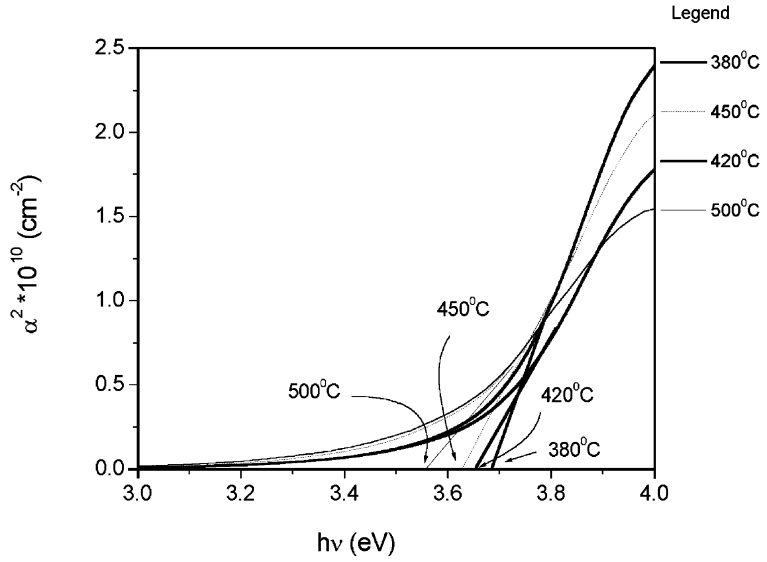

Fig. 8. α^2 vs. photon energy plots for indium oxide thin films prepared at various substrate temperatures.

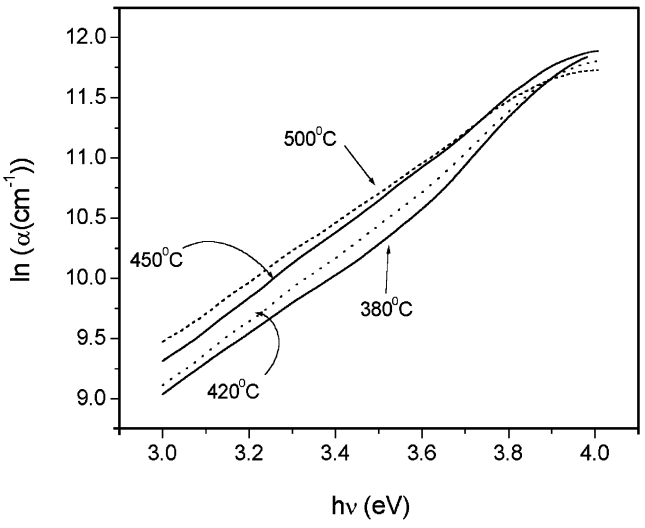

Fig. 9. Logarithm of the absorption coefficient vs. photon energy for indium oxide thin films deposited at various substrate temperatures.

transition, α^2 vs. photon energy, $h\nu$, was plotted (Fig. 8) for films deposited at different temperatures. The intercept on the x-axis gives the value of the direct band gap. Fig. 9 shows the $\ln\alpha$ vs. $h\nu$ plots for the same films. The values obtained for E_g, α_o and E_0 are presented in Table 4. The focal point is at $E_1 = 3.90$ eV.

The optical band gap values obtained (3.57–3.68 eV) are very close to the values quoted in literature [39–41].

Hamberg and Granqvist [42] shows that the band gap shift is a result of two competing mechanisms: a widening due to Burstein–Moss effect (at high electrons concentration the lowest states in the conduction band are bloked) [43], and a narrowing due to electron-ion and electron-electron scattering. The transition width—including an Urbach tail—seems to be consistent with these notions. Except the Burstein–Moss shift, the evaluation of shifts determined by the other mechanisms is still a very difficult and complex problem.

Melsheimer and Ziegler [37] suggest that the Urbach tail parameter E_0, could be a function of structural

Table 4
E_g is the optical band gap calculated using Eq. (3); α_0 is the Urbach absorption at the edge E_1 ($E_1 = 3.80$ eV) and E_0 is the Urbach energy width calculated using Eq. (4)

SI No.	T_S (°C)	Thickness (nm)	Eq. (3) 3.7–4 eV	Eq. (4) 3–3.7 eV	
			E_g (eV)	α_0 (x 10^4 cm^{-1})	E_0 (meV)
1	380	172	3.68	7.6	401
2	420	167	3.66	9.4	376
3	450	167	3.63	11.8	370
4	500	162	3.57	11.5	402

disorder and conductivity (E_0 decreases with the increase of structural order). This hypothesis is verified in our case for films deposited up to 450 °C.

Concerning the electrical conductivity (σ), for the investigated samples, σ has values between 20 and 200 Ω^{-1} cm^{-1} and increases with the increase of temperature up to ~450 °C and decrease thereafter [25].

Finally, from the presented results and other our previous observations [28], knowing that: as the temperature increase the mobility of atoms near the surface during the growing process and the chemical reaction velocity increase, we can assumed the following: at lower deposition temperature the number of oxygen vacancies is higher and consequently the concentration of free carriers is higher, as the deposition temperature increase, the structural disorder decrease and the number of oxygen vacancies decrease too, but simultaneously is expected the increase of free carriers mobility.

4. Conclusion

Highly transparent and conducting films of indium oxide have been prepared by an ultrasonic spray CVD process. The films deposited at temperature higher than 350 °C and having thicknesses greater than 100 nm are identified as polycrystalline indium oxide with a cubic structure. The increase of temperature to the range 350–500 °C improves the crystallinity. From SEM investigations results that the film grain size increase with the increasing of the temperature and the increase of thickness. The transmission in the visible and infrared regions of deposited films was found to be weakly affected by temperature deposition between 380 and 500 °C and exceed 85%. The optical band gap values ranges: 3.57–3.68 eV for films deposited at different temperatures. The plots α^2 vs. $h\nu$ indicate there is some amount of tailing in the band gap below the absorption edge. This indicates that there is a high concentration of impurity states, which can cause a perturbation of the band structure. The Urbach tail parameter E_0, was calculated for films deposited at different temperatures.

Acknowledgments

We gratefully acknowledge the support by ENSAM, Angers, France and UPR15, Pierre et Marie Curie University, Paris, France.

References

[1] C.V.R. Vasant Kumar, A.A. Mansingh, J. Appl. Phys 60 (1989) 1270.
[2] L. Tamisier, A. Carani, Electrochim. Acta 32 (1987) 1365.
[3] J.E. Costellamo, Handbook of Display Technology, Academic Press, New York, 1992.
[4] S. Ishibashi, Y. Higuchi, Y. Ota, K. Nakamuva, J. Vac. Sci. Technol. 18 (1990) 1399.
[5] K.L. Chopra, S.R. Das, Thin Film Solar Cell, Plenum Press, New York, 1983, p. 321.
[6] V.T. Bich, N.N. Dinh, T.X. Hoai, Nh. Hoang, L.V. Hong, V.D. Mien, Phys. Stat. Sol. (a) 102 (1987) K91.
[7] C. Coutal, A. Azema, J.C. Routsan, Thin Solid Films 288 (1996) 248.
[8] S. Muranaka, Thin Solid Films 221 (1992) 1.
[9] A. Salehi, Thin Solid Films 324 (1998) 214.
[10] K.F. Huang, T.M. Uen, Y.S. Gou, C.R. Huang, H.C. Yang, Thin Solid Films 148 (1987) 7.
[11] H.U. Habermeier, Thin Solid Films 80 (1981) 157.
[12] M. Mizuhaschi, Thin Solid Films 70 (1980) 91.
[13] H.J. Krokoszinski, R. Oesterlein, Thin Solid Films 187 (1990) 179.
[14] A. Hjortsberg, I. Hamberg, C.G. Granqvist, Thin Solid Films 90 (1982) 323.
[15] H.K. Muller, Phys. Stat. Sol. 27 (1968) 723.
[16] H.K. Muller, Phys. Stat. Sol. 27 (1968) 733.
[17] S. Kasiviswanathan, G. Rangarajan, J. Appl. Phys. 75 (5) (1994) 2572.
[18] G. Franksi, H. Köstlin, Phys. Stat. Sol. (a) 29 (1975) 87.
[19] S. Kulaszewicz, Thin Solid Films 76 (1981) 89.
[20] R. Pommier, C. Gril, J. Marucchi, Thin Solid Films 77 (1981) 91.
[21] M.G. Mikhailov, T.M. Ratcheva, M.D. Nanova, Thin Solid Films 146 (1987) L23.
[22] J. Dutta, P. Roubeau, T. Emeraud, J.M. Laurent, A. Smith, F. Leblanc, J. Perrin, Thin Solid Films 239 (1994) 150.
[23] M. Labeau, A.M. Gas'kov, B. Gautheron, J.P. Senateur, Thin Solid Films 248 (1994) 6.
[24] Z.B. Zhou, R.Q. Cui, Q.J. Pang, Y.D. Wang, F.Y. Meng, T.T. Sun, et al., Appl. Surf. Sci. 172 (2001) 245.
[25] M. Gîrtan, H. Cachet, G.I. Rusu, Thin Solid Films 427 (2003) 406.
[26] J. Portier, G. Campet, J. Salaerdenne, C. Marcel, C.R. Acad. Sci. Paris 322 (Serie II b) (1996) 343.
[27] J.C. Manifacier, J.P. Fillard, J.M. Bind, Thin Solid Films 77 (1981) 67.
[28] M. Gîrtan, G.I. Rusu, G.G. Rusu, S. Gurlui, Appl. Surf. Sci. 162/163 (2000) 490.
[29] M. Gîrtan, G.I. Rusu, G.G. Rusu, Mater. Sci. Eng. B 76 (2000) 156.
[30] C. Aghase, M.G. Takwale, V.G. Bhide, S. Mahamuni, S.K. Kulkarni, J. Appl. Phys. 70 (12) (1991) 7382.
[31] M. Girtan, Studies of Kinetics Phenomena of Some Oxide Semiconductors in Thin Films, Doctoral Thesis, Iasi, Romania, 2000.
[32] L.J. Meng, M.P. Santos, Appl. Surf. Sci. 120 (1997) 243.
[33] L.J. Meng, M.P. Santos, Thin Solid Films 303 (1997) 151.
[34] L.J. Meng, M.P. Santos, Thin Solid Films 322 (1998) 56.
[35] R.H. Bube, Electronic Properties of Crystalline Solids, Academic Press, London, 1974.
[36] J. Tauc, R. Grigorovici, A. Yancu, Phys. Stat. Sol. 15 (1966) 627.
[37] J. Melsheimer, D. Ziegler, Thin Solid Films 129 (1985) 35.
[38] V. Damodara Das, S. Kirupavathy, L. Damodare, J. Appl. Phys. 79 (11) (1996) 8521.

[39] H.L. Hartnagel, A.L. Dawar, A.K. Jain, C. Jagadish, Semiconducting Transparent Thin Films, Institute of Publishing, Bristol and Philadelphia, 1995.
[40] K.L Chopra, S. Major, D.K. Pandya, Thin Solid Films 102 (1983) 1.
[41] R.L. Weiher, R.P. Ley, J. Appl. Phys. 37 (1) (1966) 299.
[42] I. Hamberg, C.G. Granqvist, J. Appl. Phys. 60 (11) (1986) R123.
[43] E. Burstein, Phys. Rev. 93 (1954) 632.